

Can Dynamic Contact Angle Be Measured Using Molecular Modeling?

Ateeque Malani,¹ Anilkumar Raghavanpillai,² Ernest B Wysong,² and Gregory C Rutledge¹

¹*Department of Chemical Engineering, Massachusetts Institute of Technology, Cambridge, Massachusetts 02139, USA*

²*Experimental Station, E.I. du Pont de Nemours & Co., Wilmington, Delaware 19880, USA*

(Received 6 August 2012; published 31 October 2012)

A method is presented for determining the dynamic contact angle at the three-phase contact between a solid, a liquid, and a vapor under an applied force, using molecular simulation. The method is demonstrated using a Lennard-Jones fluid in contact with a cylindrical shell of the fcc Lennard-Jones solid. Advancing and receding contact angles and the contact angle hysteresis are reported for the first time by this approach. The increase in force required to wet fully an array of solid cylinders (*robustness*) with decreasing separation distance between cylinders is evaluated. The dynamic contact angle is characterized by partial slipping of the three phase contact line when a force is applied.

DOI: [10.1103/PhysRevLett.109.184501](https://doi.org/10.1103/PhysRevLett.109.184501)

PACS numbers: 47.55.np, 47.11.Kb, 47.55.dr, 68.08.De

The famous equation of Young predicts that the three-phase contact angle (CA) formed by a liquid in contact with a partially wetted solid surface is a balance of the solid-liquid, liquid-vapor, and solid-vapor interfacial tensions and hence should be unique for a given three phase system [1]. The Wenzel and Cassie-Baxter models each define a unique apparent contact angle (θ^*) that corresponds to a minimum free energy state when a liquid is placed in contact with a structured solid surface. However, in experiments it is often possible to observe a multitude of such three-phase contact angles, whose range is bounded dynamically by advancing and receding CAs [2]. Advancing (θ_A) and receding (θ_R) CAs refer to the contact angles formed by the leading and trailing edges of a droplet in motion across a smooth or textured surface, and bracket the apparent CA predicted by the models of Young, Wenzel, or Cassie and Baxter. Contact angle hysteresis refers to the difference, $\theta_A - \theta_R$; it is the critical parameter in determining the ease with which a droplet moves across a surface. Theoretical models generally invoke molecular level assumptions (e.g., pinning and atomic roughness) to explain these observations [3–5]. To date, assessment of this dynamic wetting behavior and the range of contact angles thus observed have eluded detailed evaluation using molecular modeling techniques.

In this Letter, we propose a simulation methodology to study both equilibrium and dynamic contact angle phenomena. The methodology is validated by comparing the equilibrium contact angle (θ_{eq}) with data reported in the literature for a model Lennard-Jones (LJ) fluid. From the dynamical study, we report for the first time advancing and receding CAs using molecular modeling. We extend the methodology to analyze the robustness factor for composite surfaces at nanoscopic length scales.

Dynamic wetting behavior is manifested in a variety of natural and man-made systems. For example, a water droplet rolling (or sliding) on a lotus leaf [6], formation of dewdrops of different shapes on a flower [7], the dryness

of a bird's feather even after immersion in water [8,9], and the skimming of striders on water surfaces [10], are a few examples of natural phenomena that have inspired the preparation of man-made superhydrophobic and self-cleaning surfaces. It is widely appreciated that both the chemistry and microstructure of these natural surfaces are important to the observed phenomena.

A problem related to the forced motion of a liquid drop on a smooth surface is the forced intrusion of liquid into a porous surface; in both cases, the limit of stability for the stationary three-phase contact line is exceeded. As early as 1970, Rijke estimated the pressure required to force water between the parallel cylindrical barbs of birds' feathers [9]. More recently Tuteja *et al.* [11,12] proposed a more general *robustness factor* to characterize the resistance to intrusion of a liquid into a porous surface. The robustness factor captures the idea of a critical pressure beyond which a stable equilibrium CA is not observed. The utility of this parameter has been demonstrated experimentally [11,12]. Similarly, in Pickering emulsions, where solid nanoparticles are used to stabilize liquid droplets, stability depends upon the self-assembly of nanoparticles at the interface of two immiscible liquids. The stability of such an emulsion can be described in terms of robustness factors using the arrangement of nanoparticles at the liquid-liquid interface [13].

To date, molecular modeling techniques have been used to evaluate equilibrium wetting behavior such as that described by the models of Young, Wenzel, or Cassie and Baxter. These techniques can be classified as (a) indirect or (b) direct in their approach to evaluating CAs. The indirect approaches use molecular simulations to evaluate the interfacial energies between pairs of phases, and then invoke Young's equation to determine an equilibrium contact angle [14–16]. While these methods allow the calculation of interfacial energies with great precision, they invoke continuum level models, and do not provide molecular level information directly at the three-phase contact line.

In the absence of a similar model for advancing and receding CAs, they are incapable of describing dynamic contact angle behavior. The correctness of using surface energies to evaluate CAs on microstructured surfaces has been contested by Gao and McCarthy [2,17]. Direct approaches, by contrast, simulate a liquid droplet of finite size and curvature in contact with a flat solid surface [18,19]. These approaches can describe the three-phase contact line with molecular level detail [20–22]; in practice, however, the very small size, and corresponding radius of curvature, of the droplets that can be modeled gives rise to large vapor pressures and other finite size effects. In principle, it is possible to study dynamic contact angles using the direct methods, e.g., by applying a set of forces in some consistent manner to the individual molecules or center of mass of the liquid droplet, but the choice of how to apportion the forces among molecules is somewhat subjective.

The method we describe here is basically a variation of the direct approach to the simulation of a three-phase contact line, in which the role of curvature of the liquid and solid surfaces is reversed. A curved solid (e.g., rod, sphere) is simulated in contact with a liquid film. At sufficiently small length scales where gravitational forces may be neglected, interfacial energies alone dictate the height at which the rod or sphere floats at the liquid-vapor interface [Fig. 1(a)]. For this reason, we call this approach the *float method*. A similar simulation was recently reported by Fan *et al.* [23] to study Pickering emulsions, but no attempt was made to extract contact angle hysteresis. For illustrative purposes, we assume henceforth a solid cylinder, but application of the method to other types of particles is straightforward.

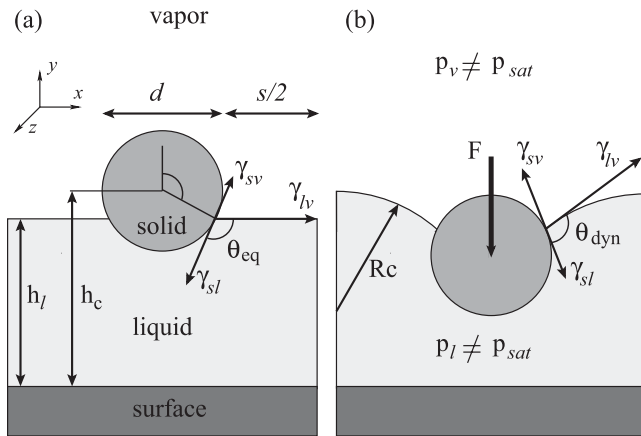


FIG. 1. Schematics of the float method to probe (a) equilibrium contact angle and (b) dynamic contact angle phenomena. The interfacial tensions (γ_{sl} , γ_{sv} , and γ_{lv}) dictate the height (h_c) of the curved solid at the liquid-vapor interface, where $\cos\theta_{eq} = 2(h_l - h_c)/d$. (b) The magnitude of applied force (F) on the curved solid establishes a new state of mechanical equilibrium by curving the liquid-vapor interface, resulting in a new, dynamic contact angle, θ_{dyn} .

The relative distance between the liquid-vapor interface (h_l) and the position of the solid cylinder (h_c) at equilibrium is related by simple geometry to the equilibrium contact angle ($\cos\theta_{eq} = 2(h_l - h_c)/d$, where d is the diameter of the cylinder). The introduction of the flat liquid-vapor interface eliminates problems such as the dependence of the vapor pressure of the liquid on droplet size (i.e., $p_l = p_v = p_{vap}$, where p_l , p_v and p_{vap} are liquid, vapor, and saturated pressure). Changes in vapor pressure with curvature of the solid cylinder are negligible. Nevertheless, care must be taken in choosing the diameter of the cylinder (d) and the separation distance (s) between periodic images of the cylinder, as discussed below.

To validate the methodology, we chose the model system of a simple LJ fluid in contact with a solid cylinder of LJ beads having (approximately) face centered cubic (fcc) crystal structure. The solid cylinder was prepared by curving a flat sheet consisting of 4 atomic layers of an fcc LJ solid with a [100] crystallographic surface, making a cylinder with 4 concentric layers [24]. Four atomic layers are sufficient to capture all solid-fluid interactions up to the cut-off distance. A schematic of the system used in simulations is shown in Fig. 1(a). Periodic boundary conditions were applied in x and z directions, and the fluid was bounded in the y direction by a reflective surface on the vapor side and a weakly attractive surface on the liquid side, to keep the liquid slab pinned to the lower half of the simulation cell. The atomic interactions were modeled using the LJ potential, $U_{ij} = 4\epsilon_{ij}[(\sigma_{ij}/r_{ij})^{12} - (\sigma_{ij}/r_{ij})^6]$, where U_{ij} is the energy of interaction, r_{ij} is the distance between two atoms and ϵ_{ij} and σ_{ij} are the energy and size parameters, respectively, of the interaction potential. Quantities made non-dimensional with respect to the fluid parameters, σ_{ff} and ϵ_{ff} are defined by superscript * [25]. To study a range of interactions between the fluid and solid ranging from wetting to nonwetting, the interaction strength between the fluid and solid molecules (ϵ_{fs}^*) was varied from 0.2 to 0.8, while the interaction distance was held constant at $\sigma_{fs}^* = 1.1$.

Molecular dynamics simulations were performed in an NVT ensemble using the LAMMPS package [26]. Temperature was maintained at $T^* = 0.9$ using the Berendsen thermostat [24]. The positions of solid beads were fixed relative to the center of mass of the cylinder, and the equations of motions were solved for the entire cylinder as a single rigid body. Results for two systems are reported here, one containing a solid cylinder with $d^* = 40$ surrounded by 13940 fluid molecules, and the other with $d^* = 44.92$ surrounded by 15383 fluid molecules. The dimensions of the simulation boxes were $L_z^* = 9.53$, $L_y^* = 117.47$ and $L_x^* = 55.31$ and 61.03 for the smaller and larger diameter cylinders, respectively. These values are large enough to avoid finite size effects associated with cylinder diameters (d) and intercylinder distances (s). The average height of the cylinder (h_c) was tracked during the

simulation. A Gibbs dividing surface methodology was used to locate the position of the liquid-vapor interface profile [$h_{lv}(x)$],

$$\int_0^{h_{lv}(x)} [\rho_l - \rho(x, y)] dy = \int_{h_{lv}(x)}^{\infty} [\rho(x, y) - \rho_v] dy,$$

where ρ_l and ρ_v are the bulk liquid and vapor densities (measured far from the interfaces), $\rho(x, y) = 1/L_z \int_0^{L_z} \rho(x, y, z) dz$ is the two dimensional density profile of fluid molecules in the system and h_l is the mean location of the liquid-vapor interface, $h_{lv}(x)$.

Figure 2(a) shows the variation in equilibrium contact angle with the strength of the fluid-solid interaction (ϵ_{fs}^*), and compares results from the current method with those reported previously in the literature for comparable LJ systems. The decrease in ϵ_{fs}^* decreases the surface energy, leading to a transition from a wetting scenario ($\cos\theta_{eq} > 0$) to a non-wetting scenario ($\cos\theta_{eq} < 0$). These results demonstrate that the float methodology reproduces the equilibrium contact angles obtained by other methods for flat surfaces. Figures 2(b) and 2(c) illustrate the density contours for $\epsilon_{fs}^* = 0.4$ and 0.7 , where we observed contact angles of $123 \pm 2^\circ$ and $63 \pm 2^\circ$, respectively. The two-dimensional density map of the fluid provides a molecularly detailed description of the three phase contact line.

To evaluate dynamic contact angles using the float method, the position of the cylinder is displaced to a fixed distance away from its equilibrium position, h_c^{eq} . Depending upon the magnitude and direction of the displacement, the three phase contact line settles to a new height on the cylinder surface. A corresponding pressure is generated within the liquid that gives rise to curvature of

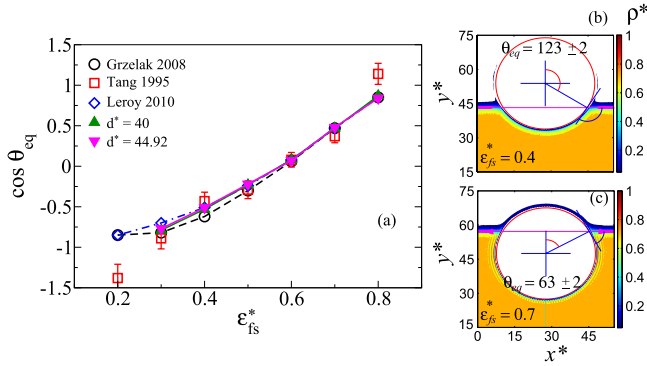


FIG. 2 (color online). (a) Wetting behavior of the LJ system with fluid-solid interaction strength ($\epsilon_{fs}^* = \epsilon_{fs}/\epsilon_{ff}$). Equilibrium contact angles are compared with data reported in the literature. (b) and (c) Two dimensional density contours of the LJ liquid in contact with the fcc-LJ solid cylinder having $\epsilon_{fs}^* = 0.4$ and 0.7 , respectively. The horizontal line indicates the location of the liquid-vapor interface, h_l . The three-phase contact lines are located where the cylinder surface and the projected liquid-vapor interface meet.

the liquid-vapor interface and formation of a new, dynamic contact angle, θ_{dyn} (Fig. 1(b)). The ensemble force (F) required to maintain the cylinder at such height was obtained unambiguously by time averaging the sum of forces exerted on all the atomic sites of the cylinder. The rest of the simulation protocol and details were identical to those used in the determination of the θ_{eq} except that the equation of motion for the cylinder was not integrated. The radius of curvature, R_c , of the liquid-vapor interface was calculated by fitting the liquid-vapor interface profile, identified by the Gibbs dividing surface, to the equation of a circle. The value of R_c can be verified independently by measuring the pressure in the liquid and vapor phases, p_l and p_v respectively, and showing that they satisfy the Young-Laplace equation. The location of the three phase contact line and θ_{dyn} were calculated by solving simultaneously the equations of two circles involving the height and diameter of the cylinder and the location and radius of curvature of the liquid-vapor interface.

Figure 3(a) shows the results for the dynamic wetting behavior of a LJ-system by molecular simulation. The variation of θ_{dyn} with F confirms that a range of contact angles exist for which the system is in mechanical equilibrium. For the advancing scenario [Fig. 1(b)], where the solid is pushed into the liquid pool, an increase in θ_{dyn} with an increase in applied force is observed, and vice versa for the receding case; this behavior is consistent with experimental observations. Slight increase beyond a critical force leads to a discontinuous transition from a partially wetted state to either complete immersion or complete detachment of the

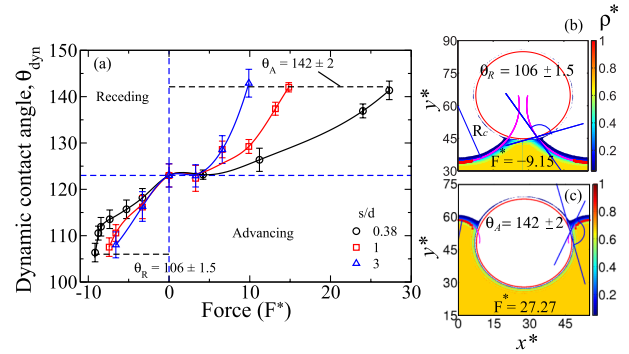


FIG. 3 (color online). (a) The variation of the dynamic contact angle of a non-wetting LJ system ($\epsilon_{fs}^* = 0.4$ and $\theta_{eq} = 123^\circ$) with the mechanical force ($F^* = F\sigma_{ff}/\epsilon_{ff}$), for three different systems having distances (s^*) 16.1, 40, and 120 between cylinders ($d^* = 40$). The horizontal dashed black lines indicate advancing (θ_A) and receding (θ_R) contact angles, beyond which a slight increase in force leads to complete wetting or de-wetting. (b) and (c) Two dimensional density map of the LJ liquid in contact with the fcc-LJ solid cylinder, illustrating the dynamic wetting phenomena at the limits of the receding and advancing scenarios respectively, for $s/d = 0.38$. The (red) data points indicate the location of liquid-vapor interface used to calculate the radius of curvature (R_c) for the liquid-vapor interface.

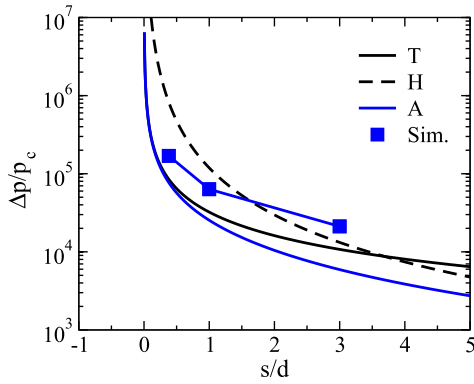


FIG. 4 (color online). Comparison of the $\Delta p/p_c$ for a nonwetting membrane ($\theta_{\text{eq}} = 123^\circ$) obtained from simulations (\square) with the robustness parameters from continuum model proposed by Tuteja *et al.* [12], considering perfect pinning (H), slipping (T) or combination of both ($1/A = 1/H + 1/T$). The simulation data points fall in between the complete pinning and complete slipping models, indicating a partial pinning scenario.

liquid from the solid cylinder, depending upon the direction of the applied force. The last points before which these transitions are observed are identified as θ_A and θ_R , respectively. For the nonwetting fluid with $\epsilon_{fs}^* = 0.4$ [Fig. 3(a)], θ_A and θ_R are observed to be 142 ± 2 and $106 \pm 1.5^\circ$, respectively, corresponding to a hysteresis of 36° .

Up to this point we have chosen d^* and s^* , just large enough to mimic equilibrium and dynamic contact angle behavior of a flat fcc solid. Through a few exploratory simulations, we observed that the continuum limit (corresponding to a flat surface) is recovered for $d^* \geq 9R_{\text{cut}}^*$ and $s^* \geq 10$, where R_{cut}^* is the range of interaction potential [27]. However, the float method readily lends itself to the study of various nanoscale systems through selection of the cylinder diameter and spacing between cylinders (e.g., nanoparticles, carbon nanotubes, and electrospun fibers). Microstructured surfaces, for example, often exhibit a metastable Cassie-Baxter equilibrium that subsequently transitions to a fully wetted, Wenzel state under applied pressure. The dynamic behavior of a liquid in contact with composite surfaces of different porosity can be studied computationally by varying the interparticle distance, s^* . We report results for three composite surfaces having interparticle distances of $s^* = 16.1, 40$ and 120 , and $d^* = 40$. The response of the dynamic contact angle to increasing force becomes more dramatic as the cylinder spacing (s^*) decreases, as evidenced by a comparison of the three curves in Fig. 3(a). For smaller s^* , the liquid-vapor interface requires a larger differential in pressure to impart a comparable shift in θ_{dyn} . Despite the differences in θ_{dyn} vs force, the θ_A and θ_R remain independent of s , confirming that they are inherent properties of the LJ system in the continuum limit. This result validates the float methodology to study dynamic wetting behavior and to calculate advancing and receding contact angles.

The increase in applied force, F^* , required to realize θ_A (or θ_R) for smaller s^* is consistent with increased resistance of such porous surfaces to liquid intrusion [11]. Here, we compare our results with the model of Tuteja *et al.* [12,24]. Estimation of the robustness factor from simulation was performed directly by calculating p_l and p_v , and dividing the difference by the capillary pressure, p_c [24]. Figure 4 compares the robustness factor of a nonwetting composite surface, having $\theta_{\text{eq}} = 123^\circ$ obtained from simulations, with that calculated by the continuum model [12]. The simulations indicate a partial pinning or slipping scenario. This is also confirmed by direct observation of the three phase contact line in the simulations. Overall, the combined model underestimates the robustness factor observed by simulation.

In summary, we have proposed and validated a new methodology that we call the *float method*, to evaluate equilibrium contact angle and contact angle hysteresis, using curved solids. The methodology opens new avenues to characterize functionalized nanoparticles, nanorods, and their assembly. The methodology is also extended to study dynamic wetting behavior of composite surfaces. For the first time, advancing and receding contact angles are reported for a model LJ system. The analysis indicates a strong dependence of wetting and de-wetting forces on microstructural parameters, yet the advancing and receding CAs remain unchanged. We also calculate the robustness factor using simulations and compare with previously reported continuum models. Though the combined model (A) underestimates the robustness factor, it can serve the purpose of initial screening in designing composite surfaces.

A. M. and G. C. R. thank Dr. Miguel Amat for useful discussion that led to this manuscript. This work was funded by the DuPont MIT Alliance.

-
- [1] A. W. Adamson and A. P. Gast, *Physical Chemistry of Surfaces* (Wiley Interscience, New York, 1997).
 - [2] L. Gao and T. J. McCarthy, *Langmuir* **25**, 14 105 (2009).
 - [3] S. P. Thampi and R. Govindarajan, *Phys. Rev. E* **84**, 046304 (2011).
 - [4] R. E. Johnson and R. H. Dettre, *Adv. Chem. Ser.* **43**, 112 (1964).
 - [5] R. H. Dettre and R. E. Johnson, *Adv. Chem. Ser.* **43**, 136 (1964).
 - [6] W. Barthlott and C. Neinhuis, *Planta* **202**, 1 (1997).
 - [7] L. Feng, Y. Zhang, J. Xi, Y. Zhu, N. Wang, F. Xia, and L. Jiang, *Langmuir* **24**, 4114 (2008).
 - [8] A. M. Rijke, *J. Exp. Biol.* **48**, 185 (1968).
 - [9] A. M. Rijke, *J. Exp. Biol.* **52**, 469 (1970).
 - [10] D. L. Hu, B. Chan, and J. W. M. Bush, *Nature (London)* **424**, 663 (2003).
 - [11] A. Tuteja, W. Choi, M. Ma, J. M. Mabry, S. A. Mazzella, G. C. Rutledge, G. H. McKinley, and R. E. Cohen, *Science* **318**, 1618 (2007).

- [12] A. Tuteja, W. Choi, J.M. Mabry, G.H. McKinley, and R.E. Cohen, *Proc. Natl. Acad. Sci. U.S.A.* **105**, 18 200 (2008).
- [13] V. Garbin, J.C. Crocker, and K.J. Stebe, *Langmuir* **28**, 1663 (2012).
- [14] J.Z. Tang and J.G. Harris, *J. Chem. Phys.* **103**, 8201 (1995).
- [15] E.M. Grzelak and J.R. Errington, *J. Chem. Phys.* **128**, 014710 (2008).
- [16] F. Leroy and F. Muller-Plathe, *J. Chem. Phys.* **133**, 044110 (2010).
- [17] L. Gao and T.J. McCarthy, *Langmuir* **23**, 3762 (2007).
- [18] T. Werder, J.H. Walther, R.L. Jaffe, T. Halicioglu, and P. Koumoutsakos, *J. Phys. Chem. B* **107**, 1345 (2003).
- [19] D. Seveno, T.D. Blake, S. Goossens, and J. De Coninck, *Langmuir* **27**, 14 958 (2011).
- [20] T. Koishi, K. Yasuoka, S. Fujikawa, and X. C. Zeng, *ACS Nano* **5**, 6834 (2011).
- [21] T.A. Ho, D. V. Papavassiliou, L.L. Lee, and A. Striolo, *Proc. Natl. Acad. Sci. U.S.A.* **108**, 16 170 (2011).
- [22] E.S. Savoy and F.A. Escobedo, *Langmuir* **28**, 3412 (2012).
- [23] H. Fan, D.E. Resasco, and A. Striolo, *Langmuir* **27**, 5264 (2011).
- [24] See Supplemental Material at <http://link.aps.org/supplemental/10.1103/PhysRevLett.109.184501> for further details.
- [25] D. Frenkel and B. Smit, *Understanding Molecular Simulation* (Academic Press, San Diego, CA, 1996).
- [26] S. Plimpton, *J. Comput. Phys.* **117**, 1 (1995).
- [27] A. Malani, M. A. Amat, A. Raghavanpillai, E. B. Wysong, and G. C. Rutledge (to be published).